Simulating tidal turbines with mesh optimisation and RANS turbulence models

Amin Abolghasemi*, Matthew D. Piggott*, Johannes Spinneken†, Axelle Viré‡ and Colin J. Cotter§
*Department of Earth Science and Engineering, Imperial College London, UK
E-mail: m.abolghasemi@ic.ac.uk
†Department of Civil and Environmental Engineering, Imperial College London, UK
‡Faculty of Aerospace Engineering, Delft University of Technology, the Netherlands
§Department of Mathematics, Imperial College London, UK

***Abstract*—A versatile numerical model for the simulation of flow past horizontal axis tidal turbines has been developed. Currently most large-scale marine models employed to study marine energy use the shallow water equations and therefore can fail to account for important turbulent physics. The model presented here is based on actuator disc momentum (ADM) theory, uses a RANS model to account for turbulence and utilises mesh optimisation in order to address the multi-scale nature of the problem. Furthermore, a series of laboratory experiments were carried out in the hydrodynamics laboratory of the Civil and Environmental Engineering Department at Imperial College London which were used to help validate the numerical model. Turbulence correction terms have been used to capture the *short circuiting of the turbulence cascade* due to the presence of the disc and thereby improve the match with the experimental data. This model has been developed with the aim that it will be seamlessly combined with larger numerical models simulating tidal flows in realistic domains, e.g. the Inner Sound of the Pentland Firth. This is where the adaptive meshing capability is a major advantage as it enables the mesh to be refined only in the locations required, thus making optimal use of limited computational resources.**

***Index Terms*—Tidal turbines, actuator disc momentum, array effects, RANS turbulence model, mesh optimisation**

I. Introduction

Global warming concerns and anxiety over fossil fuel reserves and supply security have resulted in a significant interest in renewable energy sources in the past decade. The UK has targets to produce 15% of its energy from renewable sources by 2020 [1]. Marine renewable energy (MRE) will play a vital role in helping achieve this target, but in order to maximise its potential, detailed computational fluid dynamics (CFD) investigations into the optimisation of MRE installations and the understanding and mitigation of their impacts are essential. This study focuses on the extraction of tidal stream energy from coastal waters via horizontal axis tidal turbine arrays which are currently the favoured approach to efficiently harness the vast and reliably predictable tidal resource.

The deployment of tidal turbines is a complex and expensive operation and this makes the task of locating the optimal position for such turbines even more important. Maximising power output is essential, but the environmental impacts must also be studied and modelled in depth as it is vital to ensure that the efforts to reduce the carbon footprint do not result in different environmental concerns. Previous studies have shown that in order to correctly assess the power extraction from tidal turbine arrays, an undistributed flow approach does not suffice and the hydrodynamic influences of the turbines and their wake interactions must be accounted for, [2] [3] [4] [5]. Therefore, a numerical model that aims to examine the power output and environmental impacts of tidal turbine arrays must be able to capture these features.

In the present work, initially the theoretical basis for the ADM model is presented, followed by a description of the turbulence models used and a summary of the experimental work carried out. Thereafter, verification against the Conway [6] solution for flow past an actuator disc is presented, followed by mesh optimisation results and a comparison between the numerical model and the experimental data.

II. Methodology

A. Actuator Disc Momentum theory

The 3D numerical model is based on the ADM theory outlined by Houslby et al. [7] and has been developed in Fluidity, an open source finite element CFD code with mesh optimisation capabilities [8]. ADM theory is based on the assumptions that the flow is inviscid, incompressible and isentropic with uniform inflow. The disc is infinitely thin and the thrust loading on the disc is uniformly spread. The 3D Fluidity model incorporating an ADM based representation of a turbine uses discontinuous piecewise linear functions to represent velocity and continuous piecewise quadratic functions for pressure, $\mathrm{P1_{DG}}-\mathrm{P2}$, which excels in capturing sharp jumps, such as the ones present at the location of the disc [9]. In the current model the disc is represented on the fluid mesh as a $\mathrm{P1_{DG}}$ source field where the turbine field is unity at the location of the circular disc of finite thickness and zero everywhere else in the domain. In order to set the appropriate loading on the disc, Fluidity utilises the established definition for thrust coefficient, C_T, to compute the magnitude of thrust loading that should be applied at the disc. This is uniformly spread across the volume of the disc and is therefore implemented as a momentum sink term

$$S_u = -\frac{1}{2}\rho A_{\text{disc}} C_T u_0^2, \tag{1}$$

where S_u is the momentum sink applied only at the location of the disc, ρ is the fluid density, u_0 is the unperturbed upstream velocity and A_{disc} is the disc area. u_0 can either be set equal to the inlet velocity or it can be computed using the velocity at the disc, u_{disc}, and the axial induction factor, a [10]:

$$a = \frac{1}{2}\left(1 - \left(\sqrt{1 - C_T}\right)\right), \tag{2}$$

$$u_0 = \frac{u_{\text{disc}}}{1 - a}. \tag{3}$$

The latter is the approach used in this study, where u_{disc} is calculated by computing the average velocity of the elements making up the disc. In order to validate the model, results from the numerical model have been compared and validated against the semi-analytical solution for inviscid flow past an actuator disc developed by Conway [6], as well as the simple analytical expression which gives

$$\frac{u_{\text{wake}}}{u_0} = \sqrt{1 - C_T}, \tag{4}$$

where u_{wake} is the velocity in the wake which is sufficiently far downstream from the turbine that the pressure can again be treated as uniform [7].

B. Semi-analytical solution

Conway [6] suggests an analytical form for the velocity profile of the wake behind an actuator disc and this will be used to verify the numerical ADM implementations, following a similar approach by Viré et al. [11]. Assuming, incompressible, isentropic and **inviscid** flow this takes the form

$$u_x(x,r) = u_0 - \frac{u_{\text{wake}}}{4}\left(\frac{x}{\pi\sqrt{rD/2}}Q_{-1/2}(\omega_c) + \Lambda_0(\beta_c, k_c) + 2\right) \tag{5}$$

if $r < D/2$ and

$$u_x(x,r) = u_0 - \frac{u_{\text{wake}}}{4}\left(\frac{x}{\pi\sqrt{rD/2}}Q_{-1/2}(\omega_c) + \Lambda_0(\beta_c, k_c) + 2\right) \tag{6}$$

if $r > D/2$,

where u_x is the velocity in the streamwise direction, $Q_{-1/2}(\omega_c)$ denotes the Legendre function of the second kind, $\Lambda_0(\beta_c, k_c)$ denotes Heuman's Lambda function, u_{wake} is a user input which has been computed using Eq. (4) in this study, x is the streamwise direction, r is the axial direction and D is the disc diameter with

$$\begin{aligned}
\omega_c &= (x^2 + r^2 + D^2/4)/rD, \\
k_c &= \sqrt{2rD/m_1}, \\
\beta_c &= \arcsin(x/\sqrt{m_2}), \\
m_1 &= x^2 + (D/2 + r)^2, \\
m_2 &= x^2 + (D/2 - r)^2.
\end{aligned}$$

C. Turbulence modelling

One of the main challenges when attempting to simulate flow past a turbine is the ability to correctly account for the turbulence within the flow given that ambient turbulence intensity has a significant effect on the structure of the turbine wake as demonstarted by Mycek et al. [12]. There are several approaches available for turbulence modelling. These include direct numerical simulations (DNS), large eddy simulations (LES) and turbulence models based on the Reynolds-averaged Navier-Stokes (RANS) equations. For the purpose of this study it has been decided to initially incorporate RANS turbulence models, given that their computational cost is far lower than that required with LES and nowhere near what would be required for a DNS simulation. It has been suggested that a $k - \omega$ model is better suited for modelling separating flows compared to the $k - \varepsilon$ model due to the latter's inability to capture turbulence correctly in near-wall regions [13]. Hence the original Wilcox $k - \omega$ RANS model was implemented in Fluidity. These models are based on the RANS equations, in which the velocity is decomposed into mean and fluctuating (turbulent) components

$$\rho\frac{\partial \mathbf{u}}{\partial t} + \rho\mathbf{u}\cdot\nabla\mathbf{u} = -\nabla p + \mu\nabla^2\mathbf{u} - \nabla\cdot\left(\rho\mathbf{u}'\mathbf{u}'\right), \tag{7}$$

where $\mathbf{u}$ is the mean velocity, $\mathbf{u}'$ is the fluctuating velocity, p is pressure and μ is dynamic viscosity. The final term on the right hand side, containing the Reynolds stress tensor $\rho\mathbf{u}'\mathbf{u}'$, represents the effect of turbulent fluctuations on the flow and for incompressible flows is defined as

$$\rho\mathbf{u}'\mathbf{u}' = \overline{\overline{\tau}}_R = -\frac{2}{3}k\rho\mathbf{I} + \mu_T\left(\nabla\mathbf{u} + (\nabla\mathbf{u})^{\mathrm{T}}\right), \tag{8}$$

where $k = (\mathbf{u}'\cdot\mathbf{u}')/2$ is the turbulent kinetic energy and μ_T is the dynamic eddy viscosity. The equations are closed by solving transport equations for turbulent kinetic energy, k, and turbulent frequency, ω,

$$\begin{aligned}
\rho\frac{\partial k}{\partial t} + \rho\mathbf{u}\cdot\nabla k = \nabla\cdot((\mu + \sigma^*\mu_T)\nabla k) + \overline{\overline{\tau}}_R\cdot\nabla\mathbf{u} \\
- \rho\beta^* k\omega + S_k,
\end{aligned} \tag{9}$$

$$\begin{aligned}
\rho\frac{\partial \omega}{\partial t} + \rho\mathbf{u}\cdot\nabla\omega = \nabla\cdot((\mu + \sigma\mu_T)\nabla\omega) + \alpha\left(\frac{\omega}{k}\right)\overline{\overline{\tau}}_R\cdot\nabla\mathbf{u} \\
- \rho\beta\omega^2 + S_\omega,
\end{aligned} \tag{10}$$

where σ, σ^*, β, β^* and α are the model coefficients as described in [13]. S_k and S_ω represent additional source terms which are not present in the standard $k - \omega$ RANS

model, but are included here to account for the presence of the disc. These are discussed in the next section.

D. Turbulence correction terms

The standard $k-\omega$ RANS model will tend to predict faster wake recoveries in comparison with experimental data, as demonstrated by Roc et al. [14]. This is because it fails to account for the energy transfer rate from large-scale turbulence to small-scale turbulence in the near-wake region. This is known as the *short circuiting of the turbulence cascade* due to the presence of the disc and turbulence correction terms have been suggested to capture this [15] [16] [14]. El Kasmi et al. [15] suggests an additional production term for the $k-\varepsilon$ model which is proportional to the quadratic production of turbulent kinetic energy (TKE) by shear and only applied $\pm 0.25D$ directly upstream and downstream of the disc. Rados et al. [17] extended this for the $k-\omega$ model and compute S_ω via

$$S_\omega = C_\omega \frac{1}{\rho k^2} \left(\overline{\overline{\tau}}_R \cdot \nabla \mathbf{u}\right)^2, \tag{11}$$

with $C_\omega = 4$. Rethore et al. [16] and Roc et al. [14], include additional terms for TKE, Eq. (9), as well as the dissipation production terms above. They suggest including an additional source term, $S_{k,p}$ and an additional sink term $S_{k,d}$. In this study the approach by Rethore et al. has been followed where the source and sink terms are scaled with C_T and applied only at the disc. These are calculated via

$$S_k = S_{k,p} - S_{k,d} = \frac{1}{2} C_x \left(\beta_p \mathbf{u}^3 - \beta_d \mathbf{u} \cdot k\right), \tag{12}$$

with

$$C_x = \frac{4a}{1-a}, \tag{13}$$

where $\beta_p = 0.05$ and $\beta_d = 1.5$.

E. Boundary conditions

For the comparisons against the Conway solution, the side walls, top and bottom surfaces are all set to free slip and the inlet is a Dirichlet boundary condition with constant inlet values, U_{in}, k_{in} and ω_{in}. However, when attempting to simulate realistic flows, it is important to capture the vertical asymmetry caused by the slower moving fluid near the sea bed. Hence, in the velocity field a quadratic drag boundary condition with drag coefficient $C_D = 0.0025$ is applied to the bottom surface. A zero flux boundary condition has been applied at the wall for both k and ω.

F. Laboratory experiments

A series of experiments using porous discs were carried out so that the numerical results could be validated against experimental data. The experiments utilised $15cm$ diameter porous discs and were carried out in the recirculating flume in the hydrodynamics laboratory of the Civil and Environmental Engineering Department at Imperial College London. The flume is 8m long, 1.2m wide with a depth of up to 1.1m and can support flow rates up to 200 litres per second. The methodology followed similar approaches by Harrison et al. [18], where a Nortek acoustic doppler velocimeter (ADV) was used to capture the velocity profile downstream of the disc. The ADV is capable of recording instantaneous velocity components, in three directions, at a single point. By taking advantage of the ADV's high frequency sampling rate of 200Hz, TKE and turbulence intensity (I) values can also be generated. This is valuable as the level of turbulence will have a significant effect on the wake recovery. The TKE is given by

$$k = \frac{1}{2}\left(\overline{(u_x')^2} + \overline{(u_y')^2} + \overline{(u_z')^2}\right), \tag{14}$$

where u_x' is the instantaneous turbulent velocity fluctuations in the x direction and similarly u_y' and u_z' are the components in the y and z directions respectively. I is given by

$$\mathrm{I} = \frac{u'}{U} = \frac{\sqrt{\frac{2}{3}k}}{U} \qquad \text{with} \qquad u' = \sqrt{\frac{1}{3}(u_x'^2 + u_y'^2 + u_z'^2)}, \tag{15}$$

where u' is the root mean square of the turbulent velocity fluctuations and U is the magnitude of velocity.

1) Similitude: Ensuring dynamic similitude is vital when attempting to recreate a real life scenario in a laboratory [19]. The Froude number is defined as the ratio of the characteristic fluid velocity to the gravitational wave velocity, $Fr = u/\sqrt{gd}$, where d is water depth, and it is believed that Froude similarity must be established when considering tidal turbines to ensure that the free surface at the model scale deforms in the same manner as the full-scale system

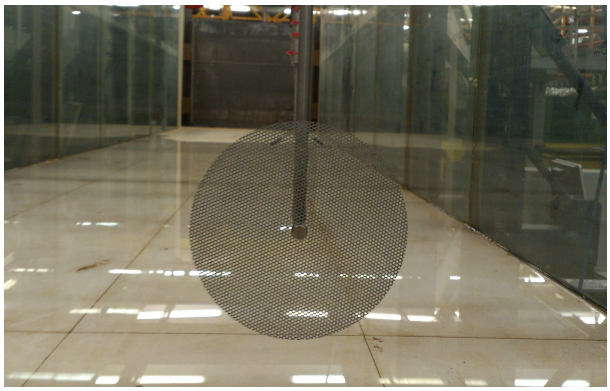

Fig. 1. An image of the porous disc inside the flume.

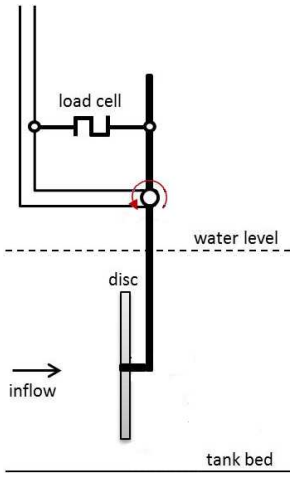

Fig. 2. Axial loading on the disc was recorded using a pivoting system.

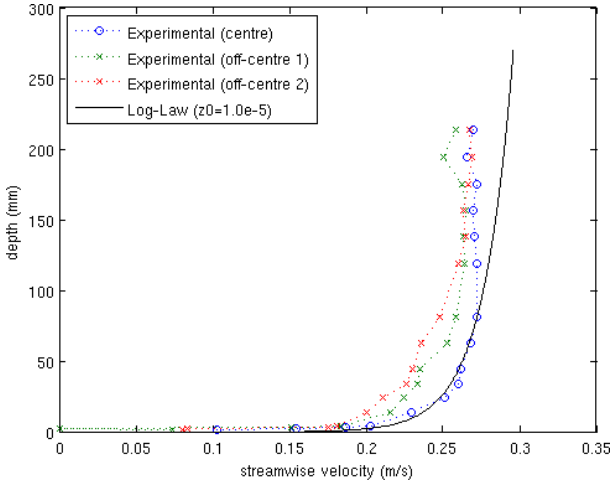

Fig. 3. Boundary layer profile: The water depth is approximately 270mm but measurements only exist up to 215mm since the ADV measures the velocity at a point 50mm below its position and only works in water. The three profiles shown correspond to one recorded in the centre of the flume and two measurements taken 30cm either side of the centre.

[18]. With this in mind and given the size of our tank, it was decided to conduct the experiments at a scale of 1:125. Table I shows how this scaling affects the other important parameters.

The rotor diameter of a real turbine is likely to be in the range of 18–20m so 18.75m is a reasonable value to consider. The real life tidal flow speed will vary sinusoidally with time and will have an estimated maximum flow speed of around $4.5ms^{-1}$. The value of $2.9ms^{-1}$ has been chosen for scaling purposes because this is roughly the velocity at which a real turbine will reach rated electric power. An important issue to note is the difference between the two Reynolds numbers. Attempting to recreate a laboratory setting where the Reynolds numbers would match is almost impossible; therefore it was decided to conduct our experiments at a sufficiently high Re such that the flow is in the turbulent regime and the value of 6.9×10^4 satisfies this criteria.

Diameter	Velocity	Water Depth	Hub Height	Fr	Re
18.75 m	2.90 ms^{-1}	33.00 m	14.0 m	0.161	9.6×10^7
0.15 m	0.26 ms^{-1}	0.264 m	0.11 m	0.161	6.9×10^4

TABLE I
EXPERIMENTAL SCALE

2) Load cell: The axial loading on the disc has to be accurately measured in order to determine its corresponding C_T. The load cell used was a FUTEK Miniature S Beam load cell and in order to ensure the correct loading is recorded, the disc was free to move in all degrees of freedom apart from the direction of interest where its motion was restricted via the load cell. The apparatus shown in Fig. 2 was used to record the axial loading and C_T was determined using

$$C_T = \frac{T}{\frac{1}{2}\rho A_{\text{disc}} u_0^2}, \tag{16}$$

where T is the axial thrust recorded. The measurements were repeated for different upstream velocity values to ensure consistency and it was determined that $C_T \approx 0.95$ for the porous disc used.

3) Resource assessment: Prior to conducting experiments in the flume it is important to understand the experimental flow conditions and so the ADV was used to measure the flow profile of the flume without the presence of any discs. Fig. 3 shows the streamwise velocity variations with depth measured at three different locations in the tank. One in the centre and two measurements taken 30cm either side of the centre which is also 30cm away from the side walls. It is therefore no surprise to see that the off-centre profiles differ from the one measured at the centre, most likely due to the viscous drag from the side walls. This non-uniformity can also be due to variations in the inlet. The following log-law can be used to fit a boundary layer profile to our data

$$u = \frac{u^*}{\kappa} \ln\left(\frac{z}{z_0}\right), \qquad u^* = \frac{u_{\text{ref}}}{\kappa} \ln\left(\frac{z_{\text{ref}}}{z_0}\right), \tag{17}$$

where $\kappa = 0.41$ and u_{ref} and z_{ref} are taken at a reference point above the flume bed. The log-law matches the lower regions of the flow, but does not provide a good match for the entire flow profile. Furthermore, the TKE measured at these locations corresponds to an ambient turbulence intensity of 5%.

III. RESULTS

A. ADM verification

Fig. 4 and Fig. 5 show streamwise ($r = 0$ and $r = D$) and radial ($x = 0$ and $x = 2D$) velocity deficit plots comparing the numerical model to the Conway solution for $C_T = 0.20$

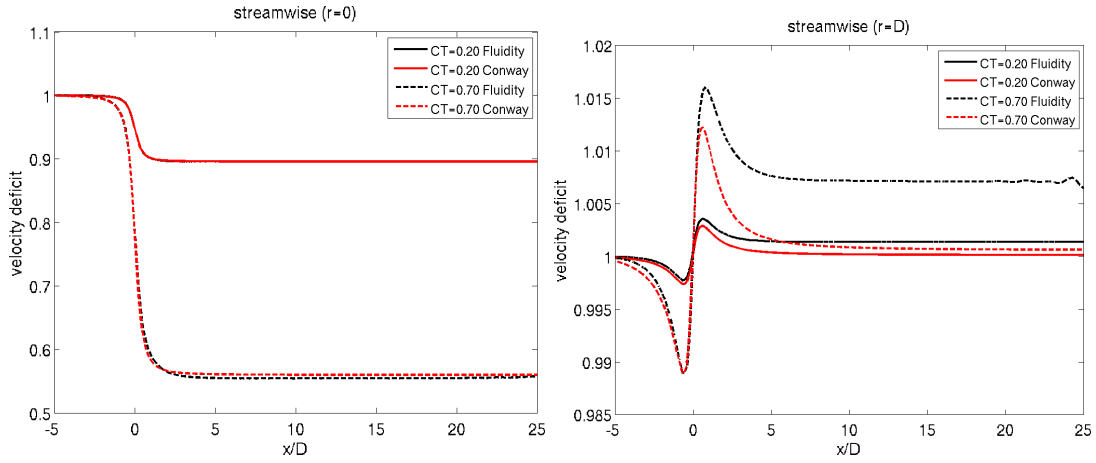

(a) streamwise velocity profile at $r = 0$ (b) streamwise velocity profile at $r = D$

Fig. 4. Streamwise comparison velocity plots at $C_T = 0.20$ and $C_T = 0.70$ with $Re = 8.4 \times 10^4$ and a domain size of $5m \times 1.2m \times 1.2m$

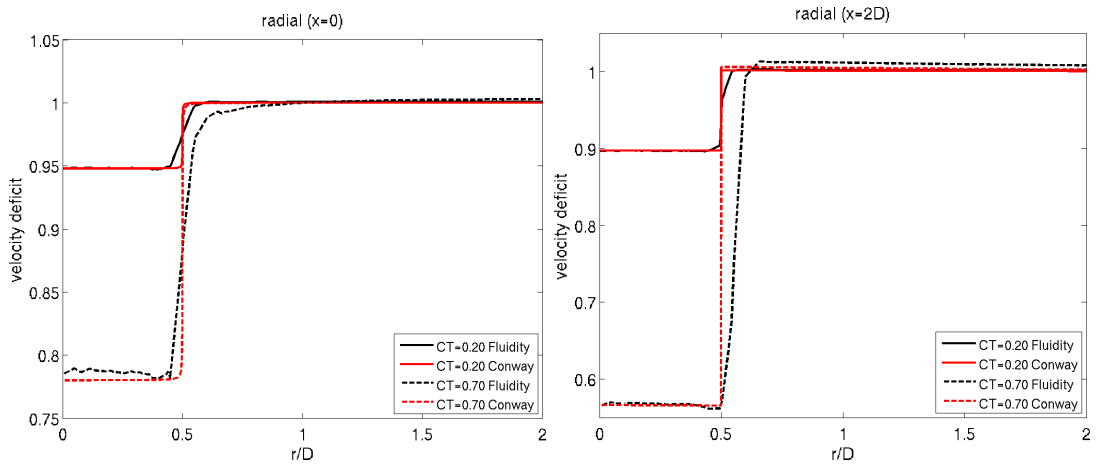

(a) radial velocity profile at $x = 0$ (b) radial velocity profile at $x = 2D$

Fig. 5. Radial comparison velocity plots at $C_T = 0.20$ and $C_T = 0.70$ with $Re = 8.4 \times 10^4$ and a domain size of $5m \times 1.2m \times 1.2m$

and $C_T = 0.70$. In order to simulate the inviscid scenario a very low kinemtaic viscosity was used, $\nu = 1 \times 10^{-6} m^2 s^{-1}$. Fig. 4(b) is the only case where the simulated results have diverged significantly from the analytical solution and this is because the analytical solution assumes an infinite domain, but the wall effect in the simulations causes the velocity outside of the wake, in the bypass region, to accelerate. This effect can be reduced by moving the walls further away from the disc; i.e. using a larger computational domain, Fig 6.

B. RANS modelling

By including the RANS turbulence model, the bypass flow is encouraged to mix with the wake and this allows the wake to re-energise. This can also be achieved by increasing the background viscosity uniformly, but this will not capture the important turbulent physics. This mixing can be visualised by the high TKE ring that develops behind the disc at the boundary between the bypass flow and the wake, Fig. 7. This region of high TKE diffuses away further downstream.

C. Mesh optimisation

The Fluidity ADM model is capable of mesh optimisation and so the mesh can be refined where necessary, e.g. locations with high velocity shear, Piggott et al. [8]. This will result in huge computational savings, especially when simulating transient flows; e.g. flood and ebb tide where the locations and nature of wakes will evolve. The adaptive mesh runs have been compared to fixed mesh runs to ensure no loss of accuracy as a result of using this feature by running both simulations until steady state was achieved, Fig. 8. A cut through the mesh used for the fixed mesh simulations is shown in Fig. 9 and the results from the adaptive mesh simulation are displayed in Fig. 10. The fixed mesh simulation used 2.4×10^5 vertices compared to only 1.0×10^5 vertices used in the adaptive simulation. Despite the computational time taken up by the adaptivity algorithms, the adaptive simulation still takes $\sim$ 32 hours compared to $\sim$ 40 hours

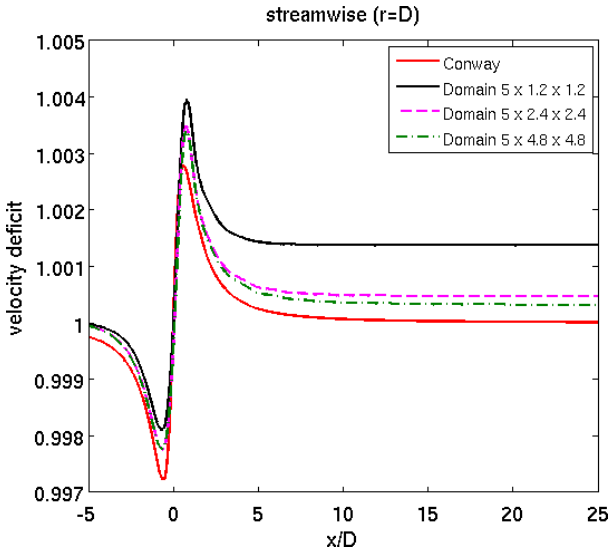

Fig. 6. Streamwise velocity profile at $r = D$ with $C_T = 0.20$ for various domain dimensions. As the domain size is increased, the wall effect is reduced and the numerical result approaches the analytical one.

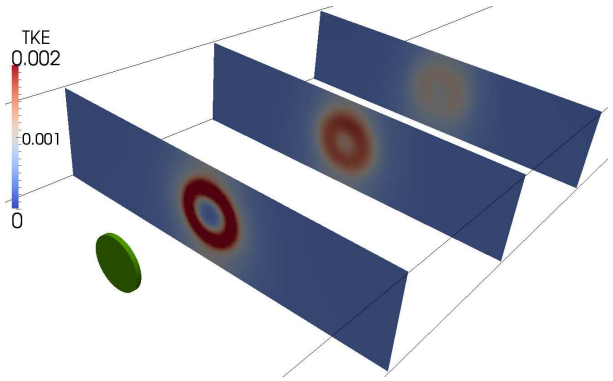

Fig. 7. The TKE downstream of the disc is shown at 2D, 6D and 10D downstream of the disc. A ring of TKE forms behind the actuator disc which dissipates away downstream as the wake recovers.

needed for the fixed simulation when both simulations were run in parallel on 16 cores. An important point to note is that in this simple case, since the location of the wake can be predicted, the mesh for the fixed mesh simulation has been carefully created and only uses a fine resolution in locations of interest. However, if the location and extent of the wake was not known, a fine resolution would have been needed throughout the domain leading to 2.0×10^6 vertices which would have taken $\sim$ 330 hours to achieve the same level accuracy as the adaptive mesh simulation. This would be further exacerbated if a longer domain and an array of turbines is employed.

D. Experimental results

Contour plots for the laboratory experiments plotted using measurements recorded on a plane at hub height are shown in Fig. 11. Measurements start at 3D downstream of the disc

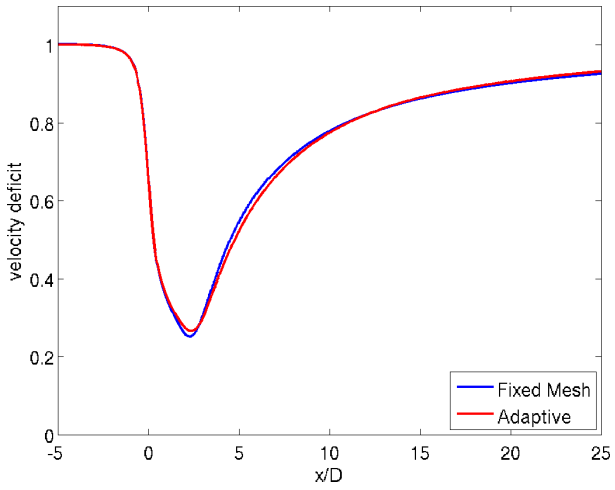

Fig. 8. A velocity deficit plot showing the results from both the fixed mesh simulation and the adaptive mesh one at $C_T = 0.99$. The domain size is $5m \times 1.2m \times 0.3m$, matching the experimental flume setup.

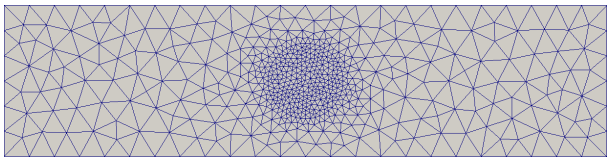

Fig. 9. Here is a cut through the mesh used for the fixed mesh simulation. This mesh has been regularly extruded in the streamwise direction with a layer thickness of $0.0125m$ which is equal to the disc thickness. Note that a finer mesh resolution is used in the centre.

up until 11.5D. Even at the furthest measured point away from the disc along the centreline, the velocity in the wake has only reached 80% of the free-stream value. The two bands of high TKE seen in Fig. 11(b) are caused by the shear layer which forms at the edges of the disc ($\pm D/2$) and extends downstream until it diffuses away as the wake starts to re-energise.

E. Comparison

It is vital to ensure that the ambient conditions of the experimental flume are maintained in the simulations. The ambient TKE as well as the velocity has to be similar to that of the flume and so the inlet values must be chosen carefully. The values $U_{\text{in}} = 0.27ms^{-1}$ and $k_{\text{in}} = 4 \times 10^{-4}m^2s^{-2}$ are chosen given that these are the recorded ambient values. ω_{in} will determine the dissipation of the inlet TKE in the streamwise direction. The working section of the flume where the disc is inserted has been chosen because it is far enough from the inlet so that the profile does not change and so the TKE values should not change significantly in the streamwise direction. High ω_{in} will result in a significant drop in the TKE in the streamwise direction and so $\omega_{\text{in}} = 0.25s^{-1}$ has been chosen to ensure that both velocity and TKE do not deviate significantly from the values specified at the inlet.

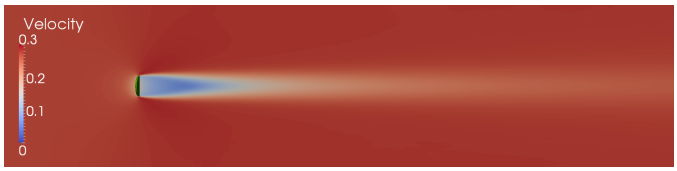

(a) velocity

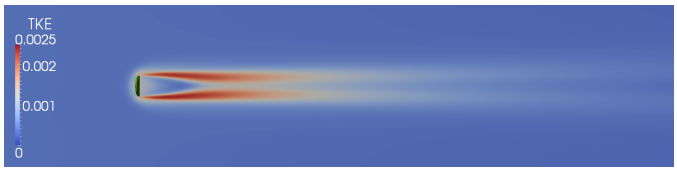

(b) TKE

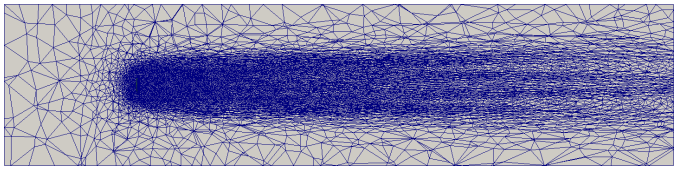

(c) adapted mesh

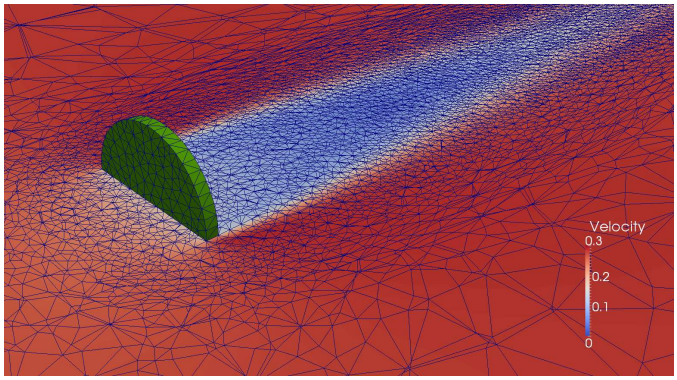

(d) a close up of the mesh near the disc

Fig. 10. During the ADM simulations, dynamic mesh adaptivity has been used to adapt to the velocity, TKE and ω fields. A 2D slice across the 3D domain is presented here showing the velocity and TKE results at hub height along with the adapted mesh.

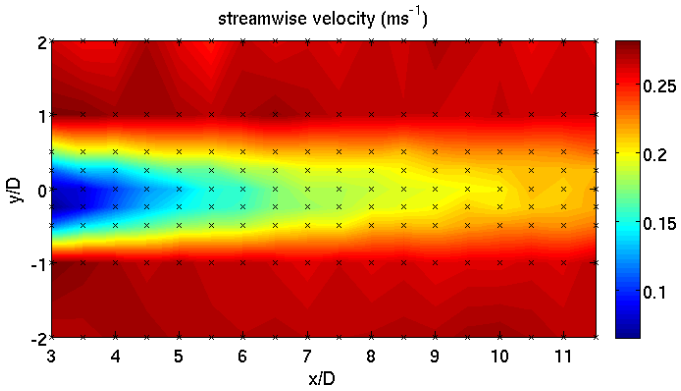

(a) velocity

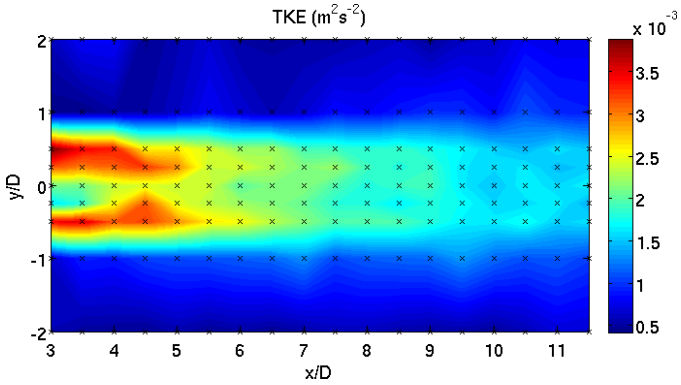

(b) TKE

Fig. 11. Contour plots showing the flow past a single 40% porous disc recorded on a plane at hub height behind the disc. X marks the locations where the ADV was used to record measurements.

Fig. 12 displays both the numerical results using the ADM Fluidity model with the modified $k-\omega$ RANS model and the flume results obtained using porous discs. It has been noticed that increasing C_ω, Eq. (11), helps improve the velocity deficit match with the experimental data by shifting the peak downstream, Fig. 12(a). This is because a higher C_ω results in increased ω which dissipates the TKE resulting in a drop in the peak TKE values, Fig. 12(b), and delays the wake recovery. Overall, the ADM model matches the velocities well and captures the correct TKE patterns, although the values are lower than the recorded experimental ones. This could be improved by applying a higher momentum sink term which would imply the disc has a C_T greater than 1. It is possible that the disc's C_T exceeds 1, because although the disc porosity of 40% is similar to that used by Harrison et al. [18], the disc used in this study has much finer holes. This suggests that a disc's C_T is not a function of porosity only, contrary to the relationship between porosity and C_T presented in Whelan et al. [20]. Furthermore, the fine hole diameter would result in greater turbulent mixing which explains the need to use a higher C_ω than Rados et al. [17] given that his study was based on wind turbines.

F. Reversing flow

In order to demonstrate the benefits of the mesh optimisation capabilities of the Fluidity ADM model, the flow direction is reversed, once steady state is reached, and the mesh consequently adapts to capture the wake which develops on the other side of the disc, Fig. 13. This can be extended to model transient flows and also flows where the flow direction will not be perfectly aligned with the disc or domain or when localised transient features such as eddies might impinge on the array.

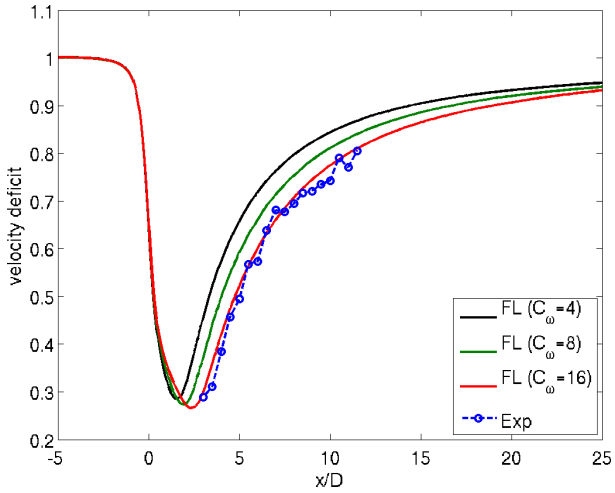

(a) velocity deficit along centerline ($r = 0$)

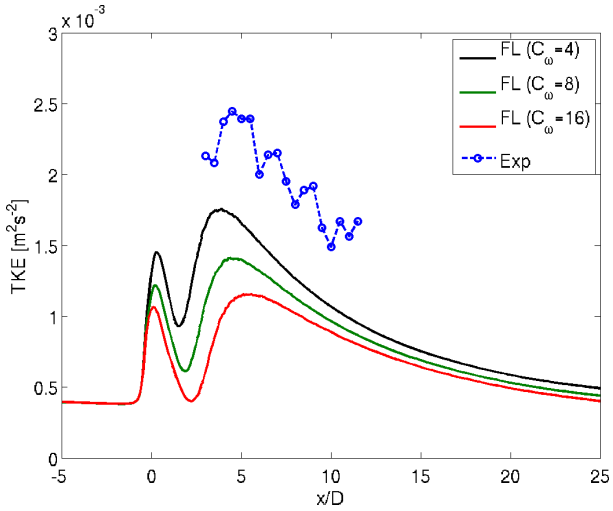

(b) TKE along centreline ($r = 0$)

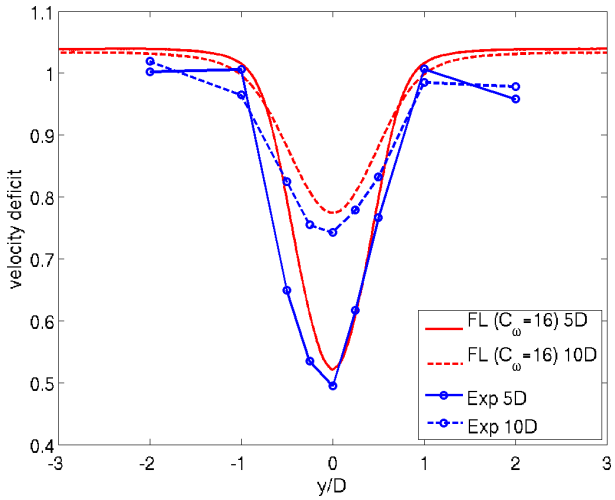

(c) velocity deficit at 5D and 10D

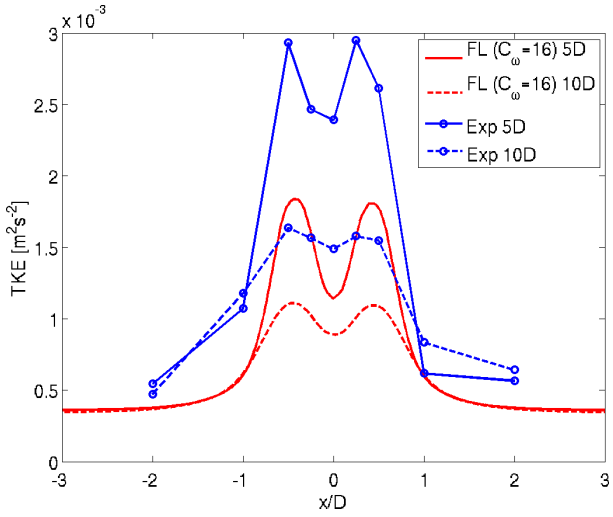

(d) TKE at 5D and 10D

Fig. 12. Experimental data vs Fluidity $k-\omega$ ADM model at $C_T = 0.99$ with different C_ω values, Eq. (11).

IV. Conclusion

An ADM model has been developed and verified which can simulate flow past horizontal axis tidal turbines and account for turbulence characteristics. The validity of the model has been assessed via a series of laboratory experiments which has provided valuable insight into the importance of accounting for the short circuiting of the turbulence cascade due to the presence of the disc when using RANS models. The versatility of the model needs to be tested via a comparison against established numerical ADM models and by attempting to simulate published experimental data for flow past scaled rotors as well as porous discs. Moreover, a comparison study of the various RANS models can help improve the experimental match.

The mesh optimisation capability of the Fluidity model means that it can be easily extended to simulate flows past multiple turbines and thus be used for assessing the power extraction and the environmental impacts of tidal turbine arrays. The next step will be to seamlessly extend this model in order to investigate flow past arrays of tidal turbines in realistic tidal flow channels where the large scale simulations will be carried out in Fluidity using a single layered model for efficiency, where 3D dynamics are unimportant, and in regions where the turbines are located the number of layers can be increased and the ADM model is inserted. Furthermore, this 3D ADM model can be used to help improve the current layout optimisation of tidal turbine arrays, developed by Funke et al. [21], which uses a shallow water model.

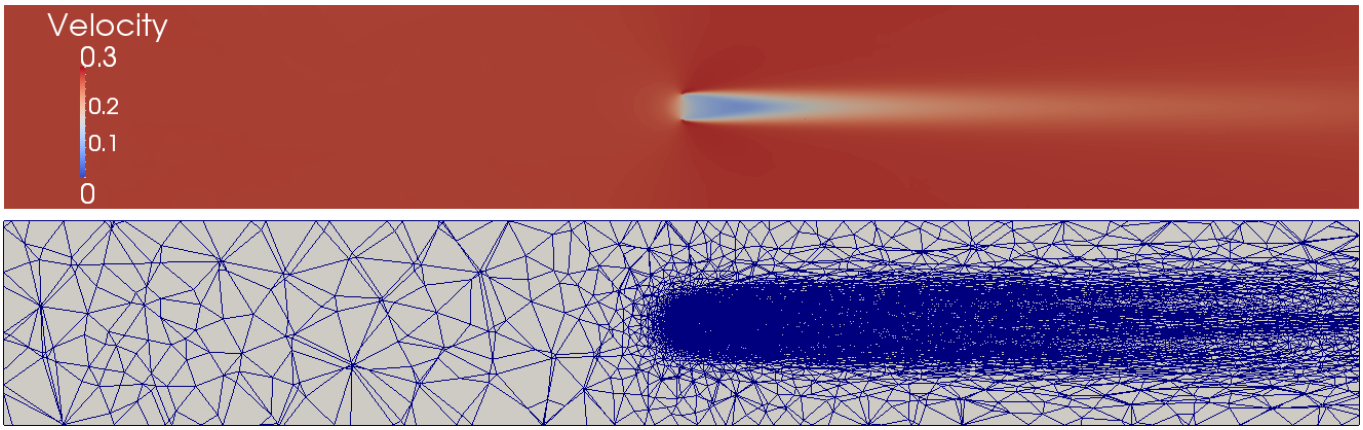

(a) steady state is reached for the flow running from left to right

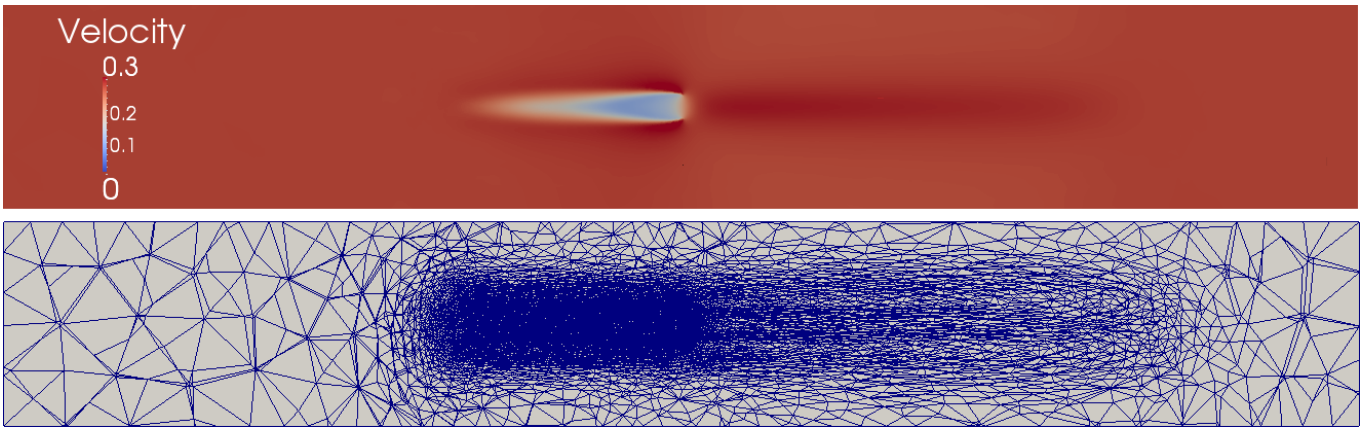

(b) flow direction is reversed and the mesh optimisation is rearranging the elements in order to capture the wake

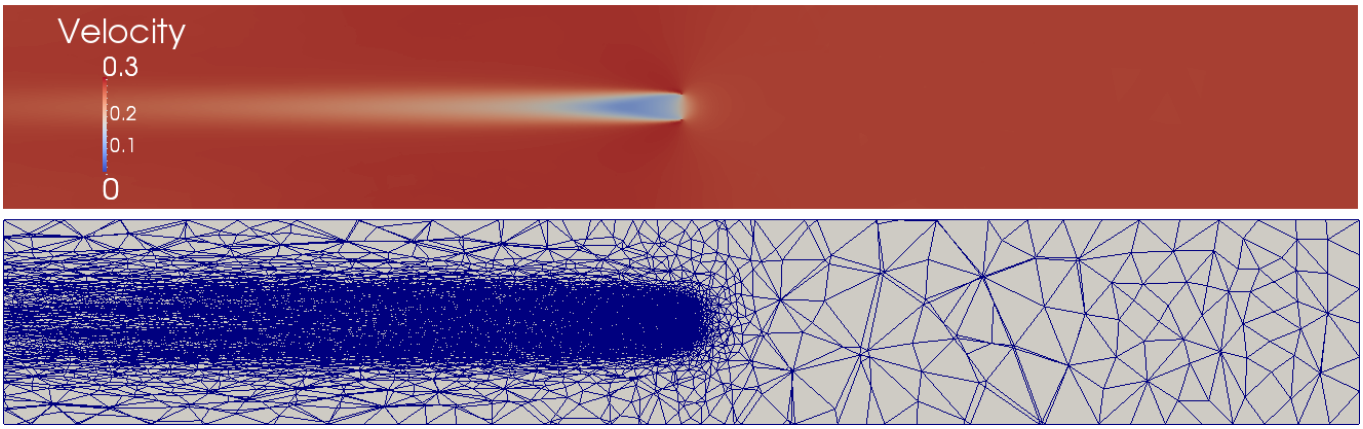

(c) steady state is reached for the flow running from right to left

Fig. 13. Fluidity ADM model's mesh optimisation provides an ideal tool to model reversing flows. 2D slices across the 3D domain are shown at several times throughout the simulation.

ACKNOWLEDGMENT

This work was supported by a studentship for the first author which has been funded by an EPSRC Industrial CASE award in collaboration with MeyGen Ltd. The authors also gratefully acknowledge the contributions of Dr. Stephan Kramer from Imperial College London and Dr. Mattias Green from Bangor University who provided support with the experimental setup.

REFERENCES

[1] THE EUROPEAN PARLIAMENT AND THE COUNCIL OF THE EUROPEAN UNION, "DIRECTIVE 2009/28/EC OF THE EUROPEAN PARLIAMENT AND OF THE COUNCIL of 23 April 2009 on the promotion of the use of energy from renewable sources and amending and subsequently repealing Directives 2001/77/EC and 2003/30/EC," 2009.

[2] C. Garrett and P. Cummins, "Generating power from tidal currents,"

Journal of waterway, port, coastal, and ocean engineering, vol. 130, no. 3, pp. 114–118, 2004.

[3] J. Whelan, J. Graham, and J. Peiro, "A free-surface and blockage correction for tidal turbines," *Journal of Fluid Mechanics*, vol. 624, no. 1, pp. 281–291, 2009.

[4] R. Vennell, "Tuning turbines in a tidal channel," *Journal of fluid mechanics*, vol. 663, no. 1, pp. 253–267, 2010.

[5] T. Nishino and R. H. Willden, "Effects of 3-D channel blockage and turbulent wake mixing on the limit of power extraction by tidal turbines," *International Journal of Heat and Fluid Flow*, vol. 37, pp. 123–135, 2012.

[6] J. T. Conway, "Analytical solutions for the actuator disk with variable radial distribution of load," *Journal of Fluid Mechanics*, vol. 297, pp. 327–355, 1995.

[7] G. Houlsby, S. Draper, M. Oldfield *et al.*, "Application of linear momentum actuator disc theory to open channel flow," *Report No. OUEL*, vol. 2296, no. 08, 2008.

[8] M. Piggott, G. Gorman, C. Pain, P. Allison, A. Candy, B. Martin, and M. Wells, "A new computational framework for multi-scale ocean modelling based on adapting unstructured meshes," *International Journal for Numerical Methods in Fluids*, vol. 56, no. 8, pp. 1003–1015, 2008.

[9] C. J. Cotter, D. A. Ham, C. C. Pain, and S. Reich, "LBB stability of a mixed galerkin finite element pair for fluid flow simulations," *Journal of Computational Physics*, vol. 228, no. 2, pp. 336–348, 2009.

[10] M. O. L. Hansen, "Aerodynamics of wind turbines," 2000.

[11] A. Viré, J. Xiang, M. Piggott, C. Cotter, and C. Pain, "Towards the fully-coupled numerical modelling of floating wind turbines," *Energy Procedia*, vol. 35, pp. 43–51, 2013.

[12] P. Mycek, B. Gaurier, G. Germain, G. Pinon, and E. Rivoalen, "Experimental study of the turbulence intensity effects on marine current turbines behaviour. Part I: One single turbine," *Renewable Energy*, vol. 66, pp. 729–746, 2014.

[13] D. C. Wilcox, *Turbulence modeling for CFD*. DCW industries La Canada, CA, 1998, vol. 2.

[14] T. Roc, D. C. Conley, and D. Greaves, "Methodology for tidal turbine representation in ocean circulation model," *Renewable Energy*, vol. 51, pp. 448–464, 2013.

[15] A. El Kasmi and C. Masson, "An extended k–ε model for turbulent flow through horizontal-axis wind turbines," *Journal of Wind Engineering and Industrial Aerodynamics*, vol. 96, no. 1, pp. 103–122, 2008.

[16] P.-E. M. Rethore, N. N. Sørensen, A. Bechmann, and F. Zahle, "Study of the atmospheric wake turbulence of a CFD actuator disc model," in *2009 European Wind Energy Conference and Exhibition*, 2009.

[17] K. Rados, J. Prospathopoulos, N. C. Stefanatos, E. Politis, P. Chaviaropoulos, and A. Zervos, "CFD modeling issues of wind turbine wakes under stable atmospheric conditions," in *European wind energy conference & exhibition proceedings, Parc Chanot, Marseille, France*, 2009, pp. 16–19.

[18] M. Harrison, W. Batten, L. Myers, and A. Bahaj, "Comparison between CFD simulations and experiments for predicting the far wake of horizontal axis tidal turbines," *Renewable Power Generation, IET*, vol. 4, no. 6, pp. 613–627, 2010.

[19] S. Hughes, *Physical models and laboratory techniques in coastal engineering*. World Scientific Publishing Company Incorporated, 1993, vol. 7.

[20] J. Whelan, M. Thomson, J. Graham, and J. Peiro, "Modelling of free surface proximity and wave induced velocities around a horizontal axis tidal stream turbine," in *Proceedings of the 7th European Wave and Tidal Energy Conference*, 2007.

[21] S. W. Funke, P. E. Farrell, and M. Piggott, "Tidal turbine array optimisation using the adjoint approach," *Renewable Energy*, vol. 63, pp. 658–673, 2014.